Applied Clay Science 210 (2021) 106156

Contents lists available at ScienceDirect

Applied Clay Science

journal homepage: www.elsevier.com/locate/clay

Note

Assessment of temperature effect on bentonite microstructure deformability

Vicente Navarro *, Gema De la Morena, Virginia Cabrera, Juan Alonso, Laura Asensio

Geoenvironmental Group, Universidad de Castilla-La Mancha, Avda. Camilo José Cela s/n, 13071 Ciudad Real, Spain

ARTICLE INFO

Keywords:
Compacted bentonite
Microstructure deformability
Temperature effects
Clausius-Clapeyron type eq.
3D-state surface

ABSTRACT

The temperature effect on the microstructure deformability of compacted bentonites was assessed using a Clausius-Clapeyron type equation. To this end, vapor adsorption data obtained at different temperatures under low water content conditions was used, identifying changes in the microstructural water with changes in the microstructural void volume. The formulation proposed allows for an extension of the 2D-models used in macroscopic double-porosity approaches to a 3D surface in which temperature is explicitly considered. The results obtained were encouraging, fitting the experimental data highly satisfactorily. Therefore, the approach proposed in this study can be a key tool for characterizing the nonisothermal behavior of compacted bentonites.

1. Introduction

As highlighted by numerous authors (Pusch, 1992; Tay et al., 2001; Acikel et al., 2020), the retention properties, low hydraulic conductivity and swelling capacity of compacted bentonites account for the keen interest in their use in different technical fields. This is particularly true in the construction of deep geological repositories for spent nuclear fuel and other high-level nuclear waste (Sellin and Leupin, 2013; Posiva, 2017), where bentonite swelling will play a key role in the potential homogenization of the system (Gens et al., 2013; Juvankoski, 2013).

In recent years, the results from microstructural testing techniques have provided important descriptive information on expansion processes (see, among others, Delage and Lefebvre, 1984; Romero and Simms, 2008; Monroy et al., 2010; Delage and Tessier, 2021), and the convenience of using multiporosity macroscopic models for simulating the behavior of compacted bentonites on an engineering scale has been highlighted. Among these models, double-porosity models (DPM) are the simplest and have undergone significant developments (see, for example, the reviews included in Mašín, 2013, and Qiao et al., 2019). These models consider the existence of two continuous media, macrostructure and microstructure. Since the seminal study by Gens and Alonso (1992), the microstructure introduces into the model the effect of the processes that occur in spaces occupied by water not flowing under hydrodynamic gradients. Fundamentally, microstructure is the space between clay layers and between the aggregates that form clay particles. In turn, the macrostructure is the tool that introduces into the soil model the effect of the processes that occur in the rest of spaces (partially saturated voids or saturated voids containing water flowing under hydrodynamic gradients).

In recent years, the application of DPM has advanced significantly, as shown by the contributions of Moyne and Murad (2003), Mainka et al. (2014) and Qiao et al. (2019) and the robust framework provided by the Barcelona Expansive Model (BExM; Alonso et al., 1999; Sánchez et al., 2005), perhaps the currently most widely used conceptual framework when developing DPM (Guimarães et al., 2013; Sánchez et al., 2016; Navarro et al., 2017a). Regardless of the macroscopic modeling strategy adopted, the changes in the microstructural void ratio, e_m (volume of microstructural voids per volume of mineral), must be modeled. Navarro et al. (2018) proposed a model in which e_m was determined as a state function of the thermodynamic swelling pressure, π, assuming that the increase in microstructure volume is equal to the increase in microstructural water. Although the model has provided satisfactory results in simulating the behavior of MX-80 under various confinement and salinity conditions (Navarro et al., 2017b; Navarro et al., 2019; Asensio et al., 2018), it did not introduce explicitly the dependence of the variation in the microstructural water content on temperature, T, which was experimentally demonstrated by Villar et al. (2006), Villar and Gómez-Espina (2007), Gailhanou et al. (2017), and Sun et al. (2020a); Fig. 1. The characterization of this dependence is a matter of interest, especially when considering the analysis of the area near the nuclear waste canister, where temperatures could reach 150 °C, according to Johnson et al. (2002).

This study analyzes the extension of the concept of π as a variable of the macroscopic state of the microstructure under nonisothermal conditions and contrasts its complementarity with temperature. For this purpose, the experimental evidence on which the analysis is based is first

* Corresponding author.
E-mail address: vicente.navarro@uclm.es (V. Navarro).

https://doi.org/10.1016/j.clay.2021.106156
Received 10 March 2021; Received in revised form 18 May 2021; Accepted 19 May 2021

described to establish the conceptual basis of the proposed formulation. Then, the scope of this formulation is assessed to illustrate the ability of the model to consistently describe the temperature effect on microstructure deformability.

2. Materials and methods

2.1. Experimental data

The findings of Villar et al. (2006) and Villar and Gómez-Espina (2007) as summarized by Jacinto (2010), as well as those of Gailhanou et al. (2017), who tested MX-80 sodium bentonites (Table 1), and of Sun et al. (2020a), who tested the Czech B75 calcium bentonite (Table 1), were analyzed. This section synthesizes the main characteristics of the previously published tests so that the reader understands how the data were collected and then analyzed. For further details, the reader is directed to each reference.

Gailhanou et al. (2017) used a thermogravimetric dynamic analyzer to determine the adsorption isotherms shown in Fig. 1 a. This figure also includes the results used by Jacinto (2010) to gather the data in Figs. 2 (a and b) and 3. These results were obtained by Villar et al. (2006) and Villar and Gómez-Espina (2007) using both the vapor equilibrium technique (see, for example, Pintado et al., 2009) and a capacitive sensor installed in a hole drilled in a bentonite block installed inside a hermetic cell. Sun et al. (2020a) (Fig. 1 b) also obtained results using the vapor equilibrium technique.

In addition, Fig. 3 plots immersion calorimetry data from Kahr et al. (1990) and Cases et al. (1992) for MX-80 bentonites. As described by Edlefsen and Anderson (1943) when analyzing the heat of wetting, immersion values increased with the enthalpy of the vaporization of water (Lide, 2005) to obtain values consistent with the enthalpy of water vapor adsorption.

2.2. Conceptual basis

Assuming that variations in the thermodynamic properties of bentonite during the water vapor adsorption process are fundamentally associated with variations experienced by the adsorbate (water) and not by the adsorbent (soil minerals), a Clausius-Clapeyron type equation (Hill, 1949) can be written to express the equilibrium

$$\left(\frac{\partial(\mathrm{Ln}\,P_V)}{\partial T}\right)_w = \frac{\Delta h}{RT^2} \tag{1}$$

where Δh is the enthalpy of water vapor adsorption, R is the universal gas constant, and the subscript w of the first term of the equation indicates that consideration is given only to those processes of variation in the absolute temperature, T, in which the gravimetric water content, w, remains constant.

The present double-porosity study assumes the differentiation of the total water content into two levels (Abed and Sołowski, 2021), analyzing the behavior of the microstructure by considering processes in which w is low enough to assume that most of the water of hydration is in the microstructure and does not form significant amounts of macro-capillary water ($w = w_m$, where w_m is the microstructural water content). According to Gailhanou et al. (2017), this occurs at a relative humidity (RH) lower than 75%, a value similar to 72% RH identified by Cases et al. (1992). According to Kelvin's law, at a temperature of 20 °C, these RH values are associated with suctions near 45 MPa, higher than the 30 MPa proposed by Jacinto et al. (2009), or the 10 MPa estimated by Villar (2007) as the suction threshold marking the flooding of macropores with capillary water. Hence, data associated with relative humidities below 80% were analyzed, obtaining e_m (Della Vecchia et al., 2013) as

$$e_m = G_S\, w_m \tag{2}$$

where G_S is the specific weight of the solid particles. Under these conditions, in Eq. [1], Δh is equal to h_V-h_m, wherein h_V is the enthalpy of water vapor and h_m is the enthalpy of microstructural water. Integrating Eq. [1] between the two temperatures T_O and T at a constant e_m, Δh can be calculated as

$$\frac{\Delta h}{R} = \frac{\mathrm{Ln}\left(P_V/P_{V,O}\right)}{(1/T_O - 1/T)} = \frac{\mathrm{Ln}\left((RH/RH_O)(P_{V0}(T)/P_{V0}(T_O))\right)}{(1/T_O - 1/T)} \tag{3}$$

where P_V defines the vapor pressure, which is equal to the product of RH and the saturation vapor pressure P_{V0} at the corresponding temperature (calculated according to the formula by Buck, 1981). Since adsorption is an exothermic process (Kahr et al., 1990), the values of Δh are positive.

The chemical potential of water in the microstructure, μ_m, can be calculated as follows (Navarro et al., 2018)

$$\mu_m = \mu_{VO}(T) + \frac{WMM}{\rho_W}(p - \pi) + \Delta\mu_{mNCC} \tag{4}$$

where μ_{VO} (T) is the chemical potential of pure water at a temperature T, WMM is the water molar mass, ρ_W is the water density and p is the net mean stress (defined as the mean stress minus the gas pressure P_G). Finally, $\Delta\mu_{mNCC}$ defines the increase in chemical potential due to the extra salinity of the microstructure. That is, the contribution to the chemical potential by cations and anions in excess of the cation exchange capacity, the non-charge-compensating ions. Assuming that water vapor behaves as an ideal gas, its chemical potential, μ_V, can be

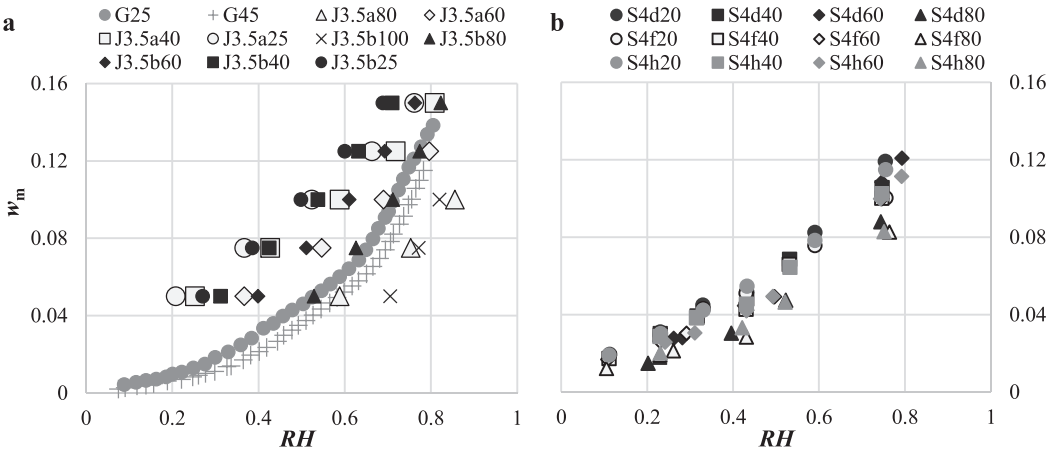

Fig. 1. Adsorption isotherms. a) MX-80 bentonites. b) B75 bentonite. Legend codes: G: Gailhanou et al. (2017), Jacinto (2010), Sun et al. (2020a); 3.a, 3.5b, 4d, 4f, 4 h: figures in the reference document where the data is presented; 20, 25, 40, 45, 60, 80, 100: T (°C).

Table 1
Main characteristics of the bentonites analyzed. I: Villar et al. (2006); II: Villar and Gómez-Espina (2007); III: Gailhanou et al. (2017); IV: Sun et al. (2020a); Mt.: Montmorillonite; Q: Quartz; F: Feldspars; C: Cristobalite; AS: Amorphous silica; [a]: Data from Gailhanou et al. (2010); [b]: Data from Sun et al. (2020b).

Bentonite	Authors	Main minerals (% weight)	Major exchangeable cations (% saturation)	Cation exchange capacity (meq/100 g)	Liquid Limit (%)	Plastic Limit (%)
MX-80	I, II	Mt 74, Q 8, F 7	Na^+ 82, Ca^{2+} 14, Mg^{2+} 4	74	350–570	70
MX-80	III	Mt 83, Q 9, C 4, AS 2	Na^+ 93, Ca^{2+} 2, K^+ 5	74[a]		
B75	IV	Mt 85	Na^+ 19, Ca^{2+} 59, Mg^{2+} 20, K^+ 2	80[b]	229	65

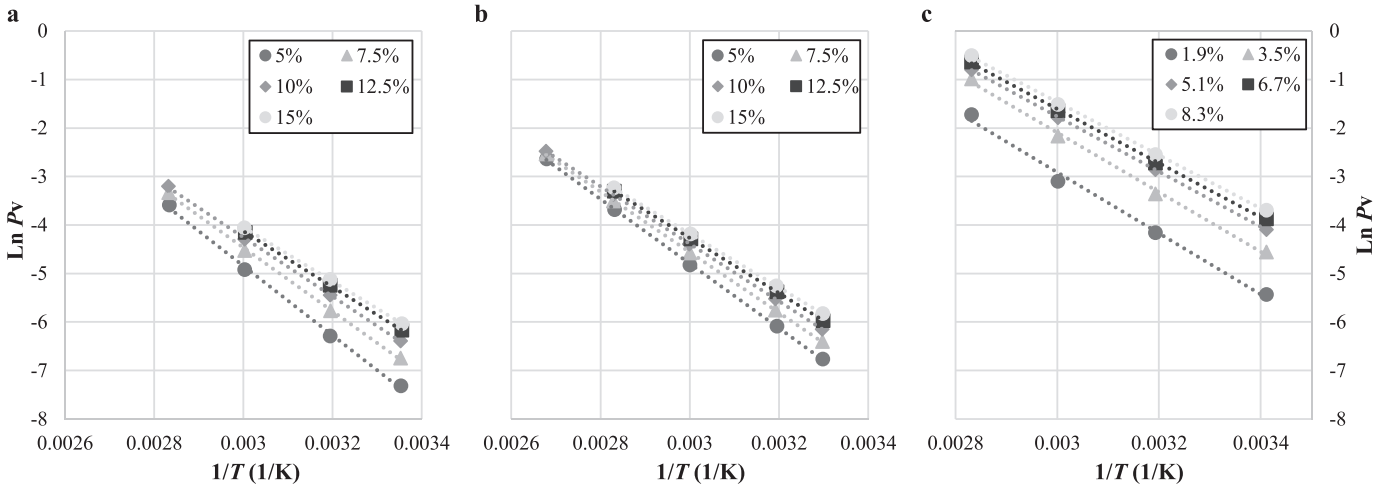

Fig. 2. a) $1/T$-Ln(P_V) relationship for the MX-80 bentonite analyzed by Jacinto (2010), dry density 1.60 g/cm^3. b) Same as a) using dry density 1.75 g/cm^3. c) $1/T$-Ln (P_V) relationship for B75 bentonite analyzed by Sun et al. (2020a). Legend: w_m values.

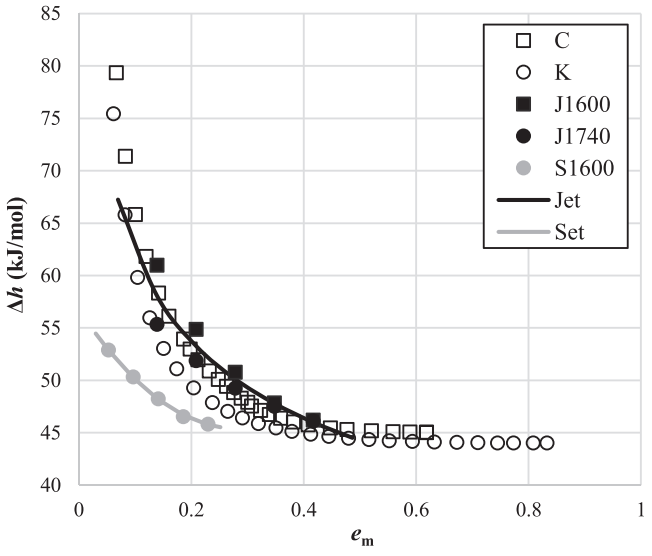

Fig. 3. Enthalpy of water vapor adsorption. C: Cases et al. (1992). K: Kahr et al. (1990). J1600: Jacinto (2010), dry density 1600 kg/m^3. J1740: Jacinto (2010), dry density 1750 kg/m^3. S1600: Sun et al. (2020a). Dry density 1600 kg/m^3. Jet: Jacinto (2010) estimated trend. Set: Sun et al. (2020a) estimated trend.

given by the following equation

$$\mu_V = \mu_{VO}(T) + RT\,\mathrm{Ln}(RH) \tag{5}$$

Therefore, when analyzing tests in which confinement is negligible, $p \approx 0$, and performed under reduced salinity conditions, $\Delta\mu_{mNCC} \approx 0$, at equilibrium, the expression

$$\pi = -\frac{\rho_W RT}{WMM}\,\mathrm{Ln}(RH) \tag{6}$$

used to convert the RH into π values holds. Using this expression, Eq. [3] can be written as

$$\pi - \frac{T}{T_O}\pi_O = \left(1 - \frac{T}{T_O}\right)\frac{\rho_W \Delta h}{WMM} + \frac{\rho_W RT}{WMM}\,\mathrm{Ln}\frac{P_{V0}}{P_{V0,O}} \tag{7}$$

Consequently, if the reference swelling pressure, π_{REF}, is defined as

$$\pi_{REF} = \frac{\rho_W \Delta h}{WMM} \tag{8}$$

then π can be calculated as

$$\pi = \pi_{REF} + \frac{T}{T_O}(\pi_O - \pi_{REF}) + \frac{\rho_W RT}{WMM}\,\mathrm{Ln}\frac{P_{V0}}{P_{V0,O}} \tag{9}$$

This is a generalized expression to calculate the thermodynamic swelling pressure π associated with the microstructural void ratio e_m at any temperature T from the value of the thermodynamic swelling pressure π_O associated with e_m at a temperature T_O.

3. Results & discussion

According to Eqs. [1] and [3], the variation in Δh with T at a constant w_m can be determined using the slope of the relationship between Ln P_V and $1/T$. Such analysis was performed using data from Jacinto (2010), Figs. 2 a and 2 b, and obtained linear functions with a Pearson coefficient of determination R^2 of almost 1. A similar result was obtained from the analysis of the data from Sun et al. (2020a) at an initial dry density of 1.60 g/cm^3, Fig. 2 c. Because the slope is constant, as implicitly assumed when integrating Eq. [1] to obtain Eq. [3], each e_m has a single Δh value, regardless of T. In Fig. 3, the resulting values were compared with the enthalpies calculated by Kahr et al. (1990) and by Cases et al. (1992).

The consistency of the comparison gives confidence to the identification of Δh and consequently to the resulting formula derived in Eq. [9].

However, the ability of Eq. [9] to predict experimental isotherms should be explicitly evaluated. For this purpose, given the quality of the data, the results of Gailhanou et al. (2017) shown in Fig. 1 were analyzed. The isotherm at 25 °C was used as the reference value π_O. The value of the thermodynamic swelling pressure "$\pi_{Eq\text{-}9}$" for 45 °C was then calculated using Eq. [9]. For this calculation, the value of π_{REF} was determined using Eq. [8], computing Δh for each value of e_m from the estimated trend of Δh identified in Fig. 3. Fig. 4 a presents the isotherms and highlights the good fit between experimental and predicted values. The goodness-of-fit is more clearly illustrated in Fig. 4 b, in which the experimental values of π (calculated using Eq. [6]) were compared with the values estimated using the model.

Highly satisfactory fits were also observed when applying the model to simulate the behavior of B75 calcium bentonite analyzed by Sun et al. (2020a). By following the procedure described in the previous paragraph, the isotherms obtained with initial dry densities of 1.27 g/cm^3 (Fig. 4 c) and 1.90 g/cm^3 (Fig. 4 e) were simulated. In both cases, the isotherm at 20 °C was taken as the reference, using the estimated trend of Δh-e_m of B75 bentonite defined in Fig. 3. Figs. 4 c and e show the isotherms at 60 and 80 °C and indicate that not only the formula is valid also for calcium bentonite but in addition applicable at temperature differences higher than the 20 °C considered in Fig. 4 a. The goodness-of-fit is shown in Figs. 4 d and f, which compare the experimental and simulated values of B75 bentonite for each isotherm.

Eq. [9] can be regarded as a 3D generalization of 2D state surfaces used in double porosity models, going from an e_m-π plane to an e_m-π-T space in which the isotherms are the contour lines of the 3D surface for constant temperatures. Thus, the isotherms of Figs. 4 c and f correspond to the three-dimensional state surfaces represented in Figs. 5 a and b, respectively.

4. Conclusions

The analysis of water vapor adsorption in the microstructure of compacted bentonites using a Clausius-Clapeyron type equation made it possible to characterize the temperature effect on the water retention capacity of the microstructure. By identifying the changes in the microstructural void volume (characterized using the microstructural void ratio e_m) with changes in the microstructural water, the formulation is a useful tool for defining microstructure deformability in double-porosity macroscopic models.

The proposed formulation was tested by comparing the experimentally measured and simulated thermodynamic swelling pressure of various MX-80 and B75 bentonites. The good fits provide confidence in the model.

Although validation of the proposed formulation should be enhanced, by analyzing its application to other bentonites and by evaluating its scope in cyclical processes of changes in water content, the formulation remains a rational and reliable strategy for extrapolating the conceptual model defined in various formulas using a 2D state surface e_m - π_M to a 3D surface e_m - π_M - T under nonisothermal conditions.

Declaration of Competing Interest

The authors declare that they have no known competing financial interests or personal relationships that could have appeared to influence

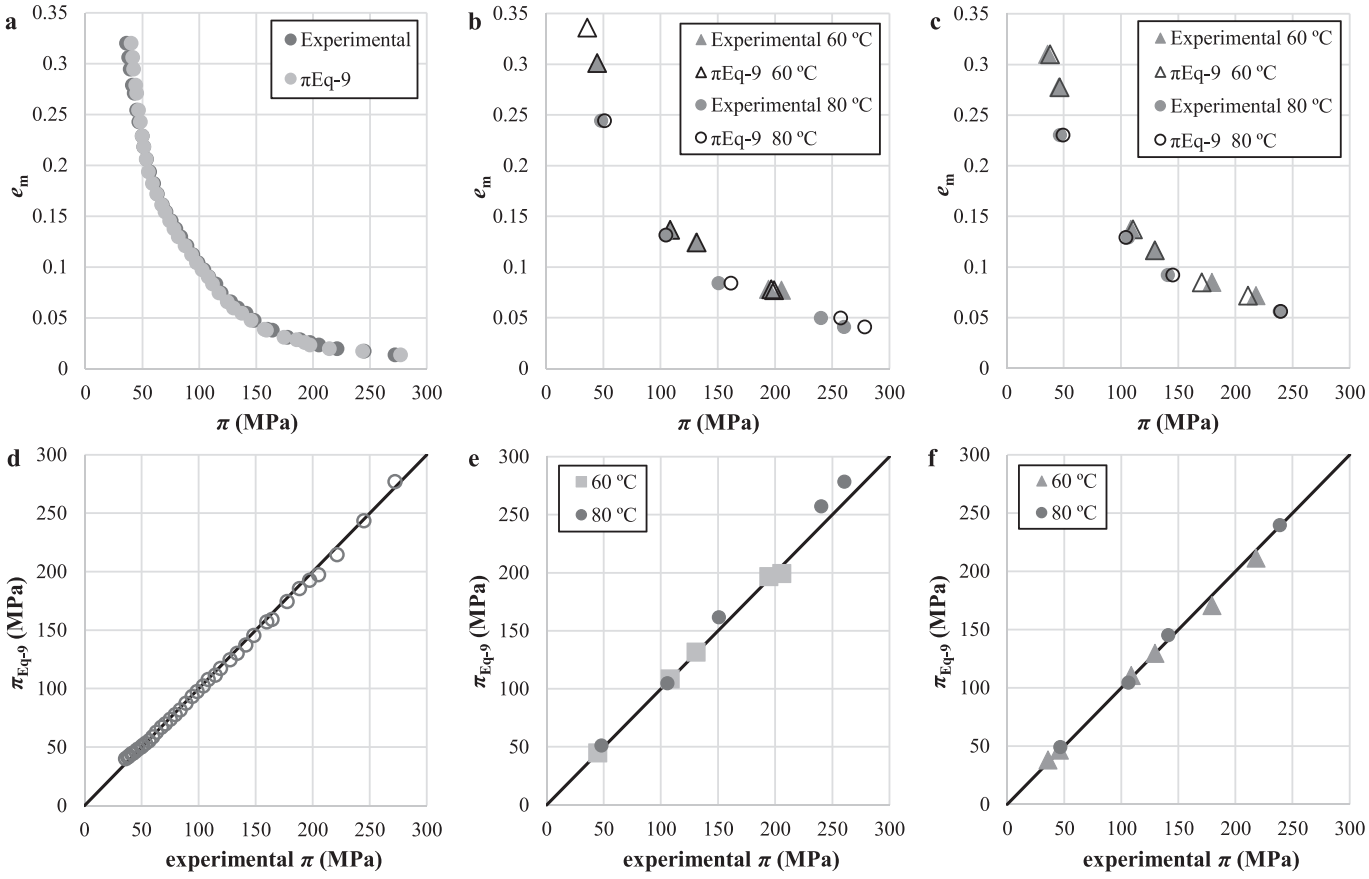

Fig. 4. Experimental and model isotherms: a) 45 °C MX-80 bentonite, Gailhanou et al. (2017); b) 60 and 80 °C B75 bentonite, dry density 1.27 g/cm^3, Sun et al. (2020a)et al. (2020 a); c) Same as b), dry density 1.90 g/cm^3. Correlation between experimental and model thermodynamic swelling pressures (line 1:1 is indicated): d) values linked to a); e), linked to b); f), linked to c).

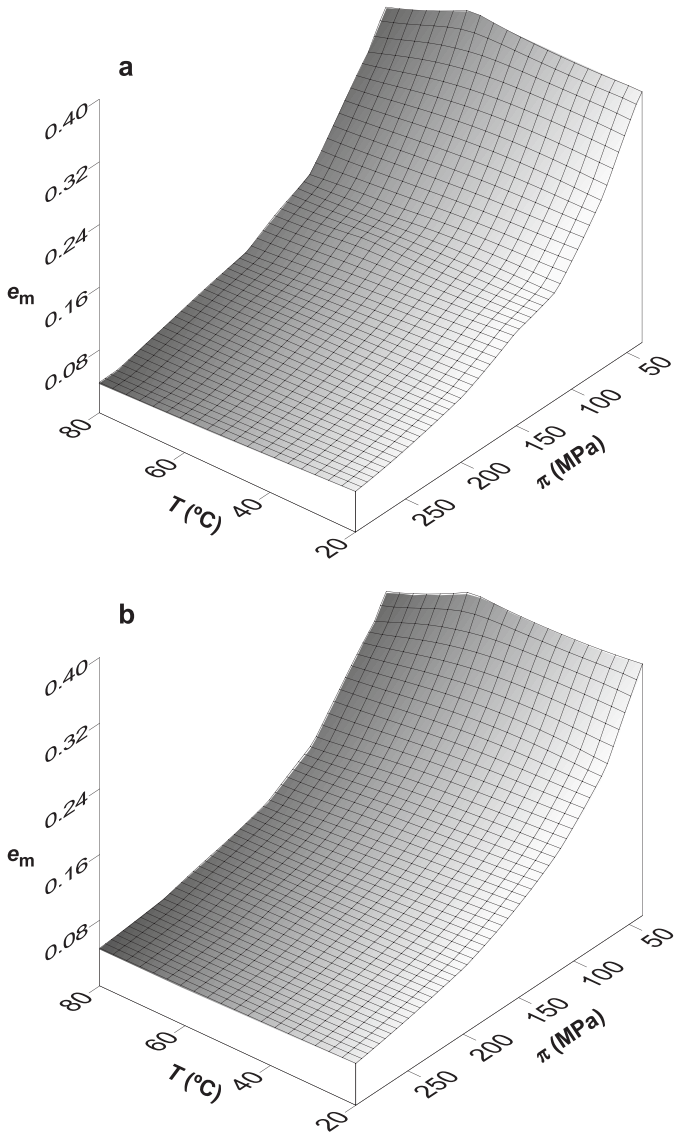

Fig. 5. 3D state surfaces e_m-π-T of B75 bentonite. a) 1.27 g/cm^3. b) 1.90 g/cm^3.

the work reported in this paper.

Acknowledgments

This study was funded by the Junta de Comunidades de Castilla-La Mancha and the European Regional Development Fund (European Union) through the project SBPLY/19/180501/000222.

References

Abed, A.A., Sołowski, W.T., 2021. Estimation of water retention behaviour of bentonite based on mineralogy and mercury intrusion porosimetry tests. Géotechnique 71 (6), 494–508. https://doi.org/10.1680/jgeot.18.P.220.

Acikel, A.S., Bouazza, A., Gates, W.P., Singh, R.M., Rowe, R.K., 2020. A novel transient gravimetric monitoring technique implemented to GCL osmotic suction control. Geotext. Geomembr. 48 (6), 755–767. https://doi.org/10.1016/j.geotexmem.2020.05.002.

Alonso, E.E., Vaunat, J., Gens, A., 1999. Modelling the mechanical behaviour of expansive clays. Eng. Geol. 54 (1–2), 173–183. https://doi.org/10.1016/S0013-7952(99)00079-4.

Asensio, L., De la Morena, G., López-Vizcaíno, R., Yustres, A., Navarro, V., 2018. Salinity effects on the erosion behaviour of MX-80 bentonite: a modelling approach. Appl. Clay Sci. 161, 494–504. https://doi.org/10.1016/j.clay.2018.05.013.

Buck, A.L., 1981. New Equations for Computing Vapor pressure and Enhancement factor. J. Appl. Meteorol. Climatol. 20 (12), 1527–1532. https://doi.org/10.1175/1520-0450(1981)020<1527:NEFCVP>2.0.CO;2.

Cases, J.M., Bérend, I., Besson, G., François, M., Uriot, J.P., Thomas, F., Poirier, J.E., 1992. Mechanism of adsorption and desorption of water vapor by homoionic montmorillonite. 1. The sodium-exchanged form. Langmuir 8 (11), 2730–2739. https://doi.org/10.1021/la00047a025.

Delage, P., Lefebvre, F.M., 1984. Study of the structure of a sensitive Champlain clay and of its evolution during consolidation. Can. Geotech. J. 21 (1), 21–35. https://doi.org/10.1139/t84-003.

Delage, P., Tessier, D., 2021. Macroscopic effects of nano and microscopic phenomena in clayey soils and clay rocks. Geomechanics for Energy and the Environment 100177. https://doi.org/10.1016/j.gete.2019.100177.

Della Vecchia, G., Jommi, C., Romero, E., 2013. A fully coupled elastic–plastic hydromechanical model for compacted soils accounting for clay activity. Int. J. Numer. Anal. Methods Geomech. 37 (5), 503–535. https://doi.org/10.1002/nag.1116.

Edlefsen, N.E., Anderson, A.B.C., 1943. Thermodynamics of soil moisture. Hilgardia 15 (2), 31–298. https://doi.org/10.3733/hilg.v15n02p031.

Gailhanou, H., Gaboreau, S., Rogez, J., Olives, J., Amouric, M., van Miltenburg, J.C., et al., 2010. Thermodynamic properties of a smectite and an illite: comparison between solubility experiments and calorimetric results. In: Clays in Natural and Engineered Barriers for Radioactive Waste Confinement – 4th International Meeting. Book of Abstracts, pp. 421–422. https://inis.iaea.org/collection/NCLCollectionStore/_Public/46/136/46136118.pdf.

Gailhanou, H., Vieillard, P., Blanc, P., Lassin, A., Denoyel, R., Bloch, E., et al., 2017. Methodology for determining the thermodynamic properties of smectite hydration. Appl. Geochem. 82, 146–163. https://doi.org/10.1016/j.apgeochem.2017.04.015.

Gens, A., Alonso, E.E., 1992. A framework for the behaviour of unsaturated expansive clays. Can. Geotech. J. 29 (6), 1013–1032. https://doi.org/10.1139/t92-120.

Gens, A., Valleján, B., Zandarín, M.T., Sánchez, M., 2013. Homogenization in clay barriers and seals: two case studies. J. Rock Mech. Geotech. Eng. 5 (3), 191–199. https://doi.org/10.1016/j.jrmge.2013.04.003.

Guimarães, L.D.N., Gens, A., Sánchez, M., Olivella, S., 2013. A chemo-mechanical constitutive model accounting for cation exchange in expansive clays. Géotechnique 63 (3), 221–234. https://doi.org/10.1680/geot.SIP13.P.012.

Hill, T.L., 1949. Statistical mechanics of adsorption. V. Thermodynamics and heat of adsorption. Journal of Chemical Physics 17 (6), 520–535. https://doi.org/10.1063/1.1747314.

Jacinto, A.C., 2010. Thermo-hydro-mechanical behaviour of expansive clays under high temperatures. In: Application to the Temperature Buffer Test Project. PhD Thesis. Departament d'Enginyeria del Terreny, Cartogràfica i Geofísica. Universitat Politècnica de Catalunya. http://hdl.handle.net/2117/93581.

Jacinto, A.C., Villar, M.V., Gómez-Espina, R., Ledesma, A., 2009. Adaptation of the van Genuchten expression to the effects of temperature and density for compacted bentonites. Appl. Clay Sci. 42, 575–582. https://doi.org/10.1016/j.clay.2008.04.001.

Johnson, L.H., Niemeyer, M., Klubertanz, G., Siegel, P., Gribi, P., 2002. Calculations of the Temperature Evolution of a Repository for Spent fuel, Vitrified High-Level Waste and Intermediate Level Waste in Opalinus Clay. Technical Report 01-04. Nagra (ISSN 1015-2636).

Juvankoski, M., 2013. Buffer design 2012. Posiva Report 2012–2014 (ISBN 978-951-652-195).

Kahr, G., Kraehenbuehl, F., Stoeckli, H.F., Muller-Vonmoos, M., 1990. Study of the water-bentonite system by vapour adsorption, immersion calorimetry and X-ray techniques. II. Heats of immersion, swelling pressures and thermodynamic properties. Clay Miner. 25 (4), 499–506. https://doi.org/10.1180/claymin.1990.025.4.08.

Lide, D.R., 2005. CRC Handbook of Chemistry and Physics, Internet Version 2005. CRC Press, Boca Raton, FL. http://www.hbcpnetbase.com.

Mainka, J., Murad, M.A., Moyne, C., Lima, S.A., 2014. A Modified Effective stress Principle for Unsaturated Swelling Clays Derived from Microstructure. Vadose Zone J. 13 (5), 1–17. https://doi.org/10.2136/vzj2013.06.0107.

Mašín, D., 2013. Double structure hydromechanical coupling formalism and a model for unsaturated expansive clays. Eng. Geol. 165, 73–88. https://doi.org/10.1016/j.enggeo.2013.05.026.

Monroy, R., Zdravkovic, L., Ridley, A., 2010. Evolution of microstructure in compacted London Clay during wetting and loading. Géotechnique 60 (2), 105–119. https://doi.org/10.1680/geot.8.P.125.

Moyne, C., Murad, M., 2003. Macroscopic Behavior of Swelling Porous Media Derived from Micromechanical Analysis. Transp. Porous Media 50 (1), 127–151. https://doi.org/10.1023/A:1020665915480.

Navarro, V., De la Morena, G., Yustres, A., González-Arteaga, J., Asensio, L., 2017a. b. Predicting the swelling pressure of MX-80 bentonite. Appl. Clay Sci. 149, 51–58. https://doi.org/10.1016/j.clay.2017.08.014.

Navarro, V., Yustres, Á., Asensio, L., De la Morena, G., González-Arteaga, J., Laurila, T., Pintado, X., 2017b. a. Modelling of compacted bentonite swelling accounting for salinity effects. Eng. Geol. 223, 48–58. https://doi.org/10.1016/j.enggeo.2017.04.016.

Navarro, V., De la Morena, G., González-Arteaga, J., Yustres, Á., Asensio, L., 2018. A microstructural effective stress definition for compacted active clays. Geomechanics for Energy and the Environment 15, 47–53. https://doi.org/10.1016/j.gete.2017.11.003.

Navarro, V., De la Morena, G., Yustres, A., López-Vizcaíno, R., Asensio, L., 2019. A Numerical Inspection on the Squeezing Test in active Clays. Géotechnique 69 (4), 329–343. https://doi.org/10.1680/jgeot.17.P.187.

Pintado, X., Lloret, A., Romero, E., 2009. Assessment of the use of the vapour equilibrium technique in controlled-suction tests. Can. Geotech. J. 46 (4), 411–423. https://doi.org/10.1139/T08-130.

Posiva, Oy, 2017. Safety Evaluation for KBS-3H Spent Nuclear fuel Repository at Olkiluoto - Description of the Disposal System. Posiva Report 2016–04 (ISBN: 978-951-652-251-0). https://www.posiva.fi/en/index/media/reports.html.

Pusch, R., 1992. Use of bentonite for isolation of radioactive waste products. Clay Miner. 27 (3), 353–361. https://doi.org/10.1180/claymin.1992.027.3.08.

Qiao, Y., Xiao, Y., Laloui, L., Ding, W., He, M., 2019. A double-structure hydromechanical constitutive model for compacted bentonite. Comput. Geotech. 115, 103173. https://doi.org/10.1016/j.compgeo.2019.103173.

Romero, E., Simms, P.H., 2008. Microstructure investigation in unsaturated soils: a review with special attention to contribution of mercury intrusion porosimetry and environmental scanning electron microscopy. Geotech. Geol. Eng. 26 (6), 705–727. https://doi.org/10.1007/s10706-008-9204-5.

Sánchez, M., Gens, A., Guimarães, L.N., Olivella, S., 2005. A double structure generalized plasticity model for expansive materials. Int. J. Numer. Anal. Methods Geomech. 29 (8), 751–787. https://doi.org/10.1002/nag.434.

Sánchez, M., Gens, A., Villar, M.V., Olivella, S., 2016. Fully coupled thermo-hydro-mechanical double-porosity formulation for unsaturated soils. International Journal of Geomechanics 16 (6). https://doi.org/10.1061/(ASCE)GM.1943-5622.0000728.

Sellin, P., Leupin, O.X., 2013. The use of clay as an engineered barrier in radioactive waste management - a review. Clay Clay Miner. 61 (6), 477–498. https://doi.org/10.1346/CCMN.2013.0610601.

Sun, H., Mašín, D., Najser, J., Scaringi, G., 2020a. Water retention of a bentonite for deep geological radioactive waste repositories: High-temperature experiments and thermodynamic modeling. Engineering Geology 269, 105549. https://doi.org/10.1016/j.enggeo.2020.105549.

Sun, H., Mašín, D., Najser, J., Neděla, V., Navrátilová, E., 2020b. Fractal characteristics of pore structure of compacted bentonite studied by ESEM and MIP methods. Acta Geotech. 15, 1655–1671. https://doi.org/10.1007/s11440-019-00857-z.

Tay, Y.Y., Stewart, D.I., Cousens, T.W., 2001. Shrinkage and desiccation cracking in bentonite–sand landfill liners. Eng. Geol. 60 (1–4), 263–274. https://doi.org/10.1016/S0013-7952(00)00107-1.

Villar, M.V., 2007. Water retention of two natural compacted bentonites. Clay Clay Miner. 55 (3), 311–322. https://doi.org/10.1346/CCMN.2007.0550307.

Villar, M.V., Gómez-Espina, R., 2007. Retention curves of two bentonites at high temperature. In: Experimental Unsaturated Soil Mechanics, 112. Springer Proceedings in Physics, pp. 267–274. https://doi.org/10.1007/3-540-69873-6_26.

Villar, M.V., Gómez-Espina, R., Martín, P.L., 2006. Behaviour of MX-80 bentonite at unsaturated conditions and under thermo-hydraulic gradient. In: Technical Report 1081, Ciemat, Madrid. http://documenta.ciemat.es/handle/123456789/777.